Engineering Structures 36 (2012) 270–282

Contents lists available at SciVerse ScienceDirect

Engineering Structures

journal homepage: www.elsevier.com/locate/engstruct

Fragility analysis of steel and concrete wind turbine towers

A. Quilligan [a], A. O'Connor [a,*], V. Pakrashi [b]

[a] Department of Civil, Structural and Environmental Engineering, Trinity College Dublin, Ireland
[b] Department of Civil and Environmental Engineering, University College Cork, Ireland

ARTICLE INFO

Article history:
Received 16 July 2011
Revised 29 November 2011
Accepted 2 December 2011
Available online 14 January 2012

Keywords:
Wind turbine towers
Concrete
Steel
Fragility curves
Lagrangian
Modal analysis
Flapwise vibration

ABSTRACT

The tower is an essential component of a wind turbine assembly with its cost amounting to approximately 30% of the overall turbine costs for onshore installations. This paper investigates the relative performance of steel and concrete tower solutions for a selection of heights and wind speeds by means of a flapwise numerical model. For each case, elements of a baseline 5 MW wind turbine are used to model the components supported by the tower. The Lagrangian approach is used to establish the equations of motion of the dynamic system, allowing for the coupling of the tower and the system of blades. The analysis is performed for a range of typical tower heights from 88 to 120 m. Comparison of the relative performance of the two tower solutions is presented using fragility curves. This illustrates the probabilistic characteristics of limit state exceedance as a function of wind loading.

1. Introduction

The current trend for wind turbines is to have larger and more powerful units, reaching higher into the atmosphere to obtain greater and more stable wind speeds. Enercon currently possess the world's largest wind turbine, E-126 [1], which is rated to 7.5 MW and sits at a hub height of 135 m. This progress towards larger turbines supported by taller towers has highlighted a number of obstacles to the traditional rolled steel tower solution. Hau [2] highlights the serious manufacturing difficulties with steel tower sections for tower heights beyond 90 m. An additional constraint is that the transportation of the lower tower sections by road is no longer feasible in many cases. In Ireland, for example, road traffic regulations specify that the maximum overall height of a vehicle may not exceed 4.65 m [3] which is unavoidable for tower heights of 90 m and above. Similar restrictions exist for most other European countries. Another aspect of steel towers at these ever increasing heights is their suitability from an economic and structural performance perspective. In view of similar structural engineering applications such as suspension and cable-stayed bridge towers it is evident that prestressed concrete and/or hybrid assemblies present an alternative, and more optimal structural solution for heights exceeding 100 m [4]. In fact, the Enercon E-126 incorporates a hybrid solution of prestressed concrete and traditional tubular steel. It is a combination of concrete's versatility in terms of transport as compared to steel, the ability to easily tune its structural properties to particular requirements and the greater service life achievable from concrete components which are influencing this movement towards hybrid and fully concrete tower solutions. A recently completed wind farm at Castledockrell in the south east of Ireland marks the emergence of concrete as a competitive tower solution with the construction of eighteen 84 m tall prestressed concrete towers [5].

Significant work has been performed to date on the dynamic modelling of wind turbine systems. Garrad [6] summarises some of the modelling techniques applied to wind turbine systems and outlines a basic Lagrangian model of the flexible tower and blade elements. Sorensen and Toft [7] outline a methodology for the probabilistic design of wind turbines to achieve high reliability and low costs. The majority of the focus, however, has been on modelling the blades and nacelle components which account for the most complex dynamic activity in the system. For example, Toft and Sorensen [8] present a probabilistic framework for the design of wind turbine blades, and Duenas-Osorio and Basu [9] employed a fragility analysis to quantify wind induced accelerations in the nacelle and their effect on acceleration-sensitive equipment. In contrast, the tower is considered a comparatively less complex component and in many cases it was seen as sufficient to ensure the tower natural frequency did not match that of the 1Ω or 3Ω frequencies, where Ω is the rotational frequency of the blades (for a 3 bladed turbine). In fact, in the case of smaller turbines it was easy to design the towers stiff enough in order to shift

* Corresponding author.
E-mail addresses: quilliga@tcd.ie (A. Quilligan), alan.oconnor@tcd.ie (A. O'Connor), v.pakrashi@ucc.ie (V. Pakrashi).

0141-0296/$ - see front matter © 2011 Elsevier Ltd. All rights reserved.
doi:10.1016/j.engstruct.2011.12.013

the eigenfrequencies beyond the excitation, as stated by Harte and Van Zijl [10]. Now, however, with the ever increasing size of wind turbine structures, understanding the dynamic response of the tower is becoming essential as the natural frequencies of tower and blades, along with the blade rotational frequency, converge.

An important component of dynamic modelling is accurate representation of the turbulent wind field. This is a topic which has been addressed in publications long before wind turbines became prominent. In reality, the most accurate means of representing a turbulent wind field is to directly solve the Navier–Stokes equations but as stated by Mann [11], "the computational costs of this would be enormous". A number of commercial finite element packages now perform this procedure through computational fluid dynamics (CFD) but even with the advances in computing power this remains a relatively time consuming process and is only valuable for fine tuning of designs which are already reasonably accurate. Most methods are, therefore, based on turbulence spectra with a particular coherence model. Kaimal et al. [12], specifically, made significant inroads on the concept of wind turbulence spectra and the findings are still very much relevant with the inclusion of the Kaimal Spectrum and Exponential Coherence Model in the European standard of wind turbine design, BS EN 61400-1 [13]. Madsen and Frandsen [14] and Connell [15] then addressed the issue of rotationally sampled turbulence and the influence of a rotating blade in a turbulent wind field. This has since been improved upon by both Veers [16], introducing an improved coherence model, and Mann [11] in which the spectral tensor for atmospheric surface layer turbulence was developed.

While some research has been conducted into wind turbine tower structures by authors such as Harte and Van Zijl [10], Bazeos et al. [17], Chen et al. [18] and Negm and Maalawi [19], there does not appear to be any examples in the literature of investigations into the structural performance of towers beyond 90 m in height in modern wind turbine installations. In particular, a comparison of the relative performance of steel and prestressed concrete as a tower solution for a variation of hub heights has not been performed to date, to the author's knowledge. There are numerous limit states under which this comparison can be made and this paper introduces the first step in this investigation.

The objective of this paper is to build on the aforementioned work within the context of identification of an optimal structural solution for tower design based upon the requirement of increasing hub heights. In this regard the relative performance of concrete and steel tower solutions for onshore wind turbines will be evaluated under varying degrees of turbulence. A probabilistic approach, employing fragility curves, is presented to facilitate this comparison. A standard rotor and turbine system is considered for a range of tower heights. The structural response of the alternative systems when subject to stochastically modelled wind loading is analysed in the flapwise direction only. With the increase in hub heights and wind turbine sizes, understanding the structural performance of the tower is becoming more important. By obtaining a more efficient solution it will not only represent an advantage in monetary terms but will result in longer structural lifespans and a more benign environment for the comparatively fragile components in the nacelle and blades.

2. Dynamic modelling

There are quite a number of design codes and simulation software packages available which model the structural behaviour of a wind turbine system. Lee et al. [20] gives an outline of these and the various methods used to solve wind turbine dynamics. For the purposes of this research a flapwise bending model of the primary flexible components of the wind turbine (blades and tower) is chosen. The most significant aspect of the model is the accurate incorporation of dynamic coupling between the rotating blades and the tower. Significant effort has been made in the development of a simplified flapwise and edgewise dynamic structural model known as the mode acceleration approach [21–23]. The transfer of shear force from the base of the blades to the tip of the tower provides basic coupling as a 2 degree of freedom (DOF) system with the resulting equation solved by the mode acceleration method [24]. The most common approach used by researchers in this area, however, is to formulate the equations of motion by the Lagrangian approach. This allows the derivation of coupling of the numerous flexible bodies (blades, tower, rotor shaft, etc.) and rigid bodies (i.e. yaw mechanism and control actuators) in two or even three dimensional space, directly minimising the total energy functions of the dynamical system [6,25]. A Lagrangian formulated model considering only flapwise vibration is developed for the tower and rotating blades in this paper and subjected to a turbulent wind loading acting solely in the out-of-plane direction of the rotor. Arrigan [26] showed the coupling effect between the blades and nacelle/tower is significantly weaker in the edgewise case than in the flapwise case. Consequently, edgewise vibration is not considered in this study. Including edgewise vibration would probably increase the accuracy of the model, however, the impact would be similar for both the concrete and steel towers considered and would not affect any of the results presented in this paper. These considerations provide the justification for the approach to model development outlined in the next section.

2.1. Lagrangian model

Hansen [25] outlines a Lagrangian formulation which provides the basis for the simplified flapwise-only model. A similar model was employed by Arrigan et al. [27] in an investigation of the vibration control of wind turbine blades. The Lagrangian formulation of the dynamic equations of motion, as defined in [28], may be expressed as follows:

$$\frac{d}{dt}\left(\frac{dT}{d\dot{q}_i}\right) - \frac{dT}{dq_i} + \frac{dV}{dq_i} = Q_i \tag{1}$$

where T is the kinetic energy of the system, V is the potential energy of the system, q_i is the displacement, $\dot{q}_i$ is the velocity and Q_i is the generalised loading corresponding to degree of freedom i. This approach allows all elements of coupling to be accurately referenced in the system of differential equations describing the dynamics.

The proposed flapwise system is illustrated in Fig. 1. The model includes two coordinate frames of reference, a local co-rotating system for each blade (x, y, z) and a global system for the combined elements which includes the tower and nacelle (X, Y, Z). At the root of each blade exists the origin of the local blade system. In Fig. 1 the orientation of the local axes, but not the origin, are shown at the tip of the blade. Wind loading is solely considered in the global X-direction as significantly less loading occurs in the other directions [13].

As already stated, in this particular model only motion in the direction of the x-axis is considered. Axial and rotational vibrations of the tower are neglected as the most important vibration interaction occurs between the exciting rotor forces and the tower bending frequencies [2].

The tower is discretised into lumped masses or nodes. As the simulations are carried out within the range of operational wind speeds of the turbine it is assumed that displacements are small and, therefore, only linear displacements without p-delta effects are considered. This allows for an eigenvalue analysis for the free vibration condition of the tower assembly. The blades are also discretised into lumped masses. Due to the rotation of the rotor,

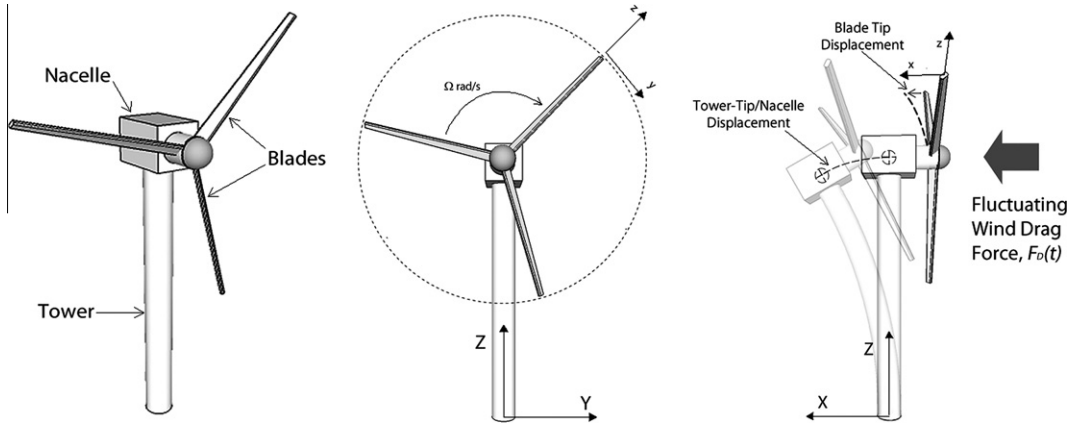

Fig. 1. Sketch of flapwise model and coordinate axes.

however, the blades afford a more comprehensive solution. This is achieved by implementing a geometric stiffness matrix to account for additional centrifugal stiffening due to blade rotation. The matrix is assembled using the formula for centrifugal stiffness outlined by Naguleswaran [29]. The resulting mass and stiffness matrices may then be implemented in an eigenvalue analysis. Accurate natural frequencies and modeshapes of the blades are produced from this method. The motion of the tower and blades in the proposed model may then be considered as a summation of the products of the calculated modeshapes $\phi_i(z)$ and the corresponding temporal tip displacements $q_i(t)$ for each particular mode i in the general form, as follows:

$$u(z,t) = \sum_{i=1}^{I} [\phi_i(z) \times q_i(t)] \tag{2}$$

The total kinetic energy of the tower is considered as the motion of the centre of mass of the tower and may, therefore, be expressed for an arbitrary number of modes J as:

$$T_T = \frac{1}{2} M_T \sum_{j=1}^{J} \left[\phi_{Tj}(CM) \times \dot{q}_{Tj}(t)\right]^2 \tag{3}$$

where M_T is the total mass of the tower, $\dot{q}_{Tj}(t)$ which is a function of time, is the modal velocity of the tower for mode j and $\phi_{Tj}(CM)$ is the value of the jth modeshape of the tower at its centre of mass (CM). Similarly, the kinetic energy of a single blade, where the overall motion of the CM of the blade may be expressed as a sum of the motion of the blade relative to the top of the tower and the tower motion, as follows:

$$\dot{v}_{CM,B} = \sum_{n=1}^{N} [\phi_{B\_n}(CM) \times \dot{q}_{B\_n}(t)] + \sum_{j=1}^{J} \left[\phi_{Tj}(tip) \times \dot{q}_{Tj}(t)\right] \tag{4}$$

may be described by:

$$T_B = \frac{1}{2} M_B \sum_{n=1}^{N} \left[\phi^2_{B\_n}(CM) \times \dot{q}^2_{B\_n}(t)\right] + 2 \sum_{n=1}^{N} [\phi_{B\_n}(CM) \times \dot{q}_{B\_n}(t)] \times \sum_{j=1}^{J} \left[\phi_{Tj}(tip) \times \dot{q}_{Tj}(t)\right] + \sum_{j=1}^{J} \left[\phi_{Tj}(tip) \times \dot{q}_{Tj}(t)\right]^2 \tag{5}$$

where M_B is the total mass of the blade, $\dot{q}_{B\_n}(t)$ is the modal velocity of the blade for mode n, $\phi_{B\_n}(CM)$ is the value of the nth modeshape of the blade at its CM, and $\phi_{Tj}(tip)$ is the value of the jth modeshape at the tip of the tower. The motion of the nacelle is also incorporated into the above kinetic energy formulation as:

$$T_{NAC} = \frac{1}{2} M_{NAC} \sum_{j=1}^{J} \left[\phi_{Tj}(tip) \times \dot{q}_{Tj}(t)\right]^2 \tag{6}$$

where M_{NAC} is the total mass of the nacelle. The total kinetic energy of the system can be shown to be:

$$T_{TOTAL} = \frac{1}{2} \sum_{i=1}^{3} M_{Bi} \left\{ \sum_{n=1}^{N} \left[\phi^2_{Bi\_n}(CM) \times \dot{q}^2_{Bi\_n}(t)\right] + 2 \sum_{n=1}^{N} [\phi_{Bi\_n}(CM) \times \dot{q}_{Bi\_n}(t)] \times \sum_{j=1}^{J} \left[\phi_{Tj}(tip) \times \dot{q}_{Tj}(t)\right] + \sum_{j=1}^{J} \left[\phi_{Tj}(tip) \times \dot{q}_{Tj}(t)\right]^2 \right\} + \frac{1}{2} M_{NAC} \sum_{j=1}^{j} \left[\phi_{Tj}(tip) \times \dot{q}_{Tj}(t)\right]^2 + \frac{1}{2} M_T \sum_{j=1}^{J} \left[\phi_{Tj}(CM) \times \dot{q}_{Tj}(t)\right]^2 \tag{7}$$

Likewise, the total potential energy of the elements of the system can be evaluated as:

$$V_{TOTAL} = \frac{1}{2} \sum_{i=1}^{3} \left\{ \sum_{n=1}^{N} \left[k_{Bi\_n} \times q^2_{Bi\_n}(t)\right] + V_{C_{Bi}} \right\} + \frac{1}{2} \times \sum_{j=1}^{J} \left[k_{Tj} \times q^2_{Tj}(t)\right] \tag{8}$$

where k_{Tj} and k_{Bi_n} are the modal stiffness's and q_{Tj} and q_{Bi_n} are the modal displacements of the tower and blade, respectively. V_C represents the additional stiffness induced in a blade due to its rotation about the hub. The effect of this rotation is twofold. The first component is centrifugal stiffening, i.e. the effect of increased stiffness of the blades induced by the rotation of the blades about the hub. The consequences of centrifugal stiffening have been proven in previous literature [29–31] to be significant and it is therefore included in this model. As the blade rotates in its vertical plane it is also affected by a varying gravity field. As seen in [21], however, the effect of gravity on the natural frequency of a rotating blade is negligible as compared to centrifugal stiffening, and is therefore not accounted for here.

The formula specified by Hansen [25], and used by Arrigan [26,27], for the centrifugal tension distribution throughout a rotating cantilever beam results in the potential energy term due to centrifugal body forces being approximated, for flapwise motion, as:

$$V_C = \frac{1}{2} \Omega^2 \int_0^L \left(\sum_{n=1}^{N} \left[q_n \times \frac{d(\phi_{B\_n}(x))}{dx} \right] \right)^2 \times \int_x^L m(\xi) d\xi dx \tag{9}$$

where Ω is the blade rotational frequency in (rad/s), L is the total length of the blade and $m(\xi)$ is the mass per unit length of the blade (kg/m).

Evaluating the expressions for the potential and kinetic energy of the system, Eq. (3)–(9), and then substituting them into the

Lagrangian formulation from Eq. (1) the equations of motion for the flapwise vibration of the system acquire the form:

$$[M]\{\ddot{q}(t)\} + [C]\{\dot{q}(t)\} + [K]\{q(t)\} = \{P(t)\} \tag{10}$$

when damping for the system is formulated as stiffness proportional damping and is specified based on the particular tower and blades being modelled [32]. Having formulated the Lagrangian model to solve the complex system the next stage in the analysis is the computation of the time dependent loading $\{P(t)\}$.

2.2. Wind loading

As the wind passes through a wind turbine it generates both a lift and drag force. The lift force is utilised as the main driving force of the blades and acts in the plane of rotation of the blades whereas the drag force acts in the plane parallel to the primary wind flow and therefore in the flapwise direction of the blades. For the purposes of the model presented here, only the drag force is considered. The drag force loading transferred to a structure of transformed area A in the path of a mass of air of density ρ moving at velocity $V(t)$, as given by [33] is

$$F_D(t) = \frac{1}{2} C_D \rho A [V(t)]^2 \tag{11}$$

where C_D is the drag coefficient. $V(t)$ may be further broken down into its mean and fluctuating components, $\overline{V}$ and $v\prime(t)$, respectively. The mean and fluctuating drag force components may subsequently be expressed as:

$$\overline{F}_D(t) = \frac{1}{2} C_D \rho A \overline{V}^2 \tag{12}$$

and

$$F\prime_D(t) = \frac{1}{2} C_D \rho A \left\{ 2\overline{V} v\prime(t) + v\prime(t)^2 \right\} \tag{13}$$

respectively. The fluctuating velocity time histories, $v\prime(t)$, are generated as a Fourier series using the approach utilised by Murtagh et al. [34]. The Fourier coefficients are established from a specific Power Spectral Density Function (PSDF) as normally distributed random numbers with zero mean and standard deviation σ_i, where σ_i is equal to the area under the PSDF between the frequency limits f_i and $f_i + df$. The Kaimal spectrum as specified in Annex B of BS EN 61400-1 [13] is used in this analysis and it may be represented as follows:

$$\frac{fS_k(f)}{\sigma_k^2} = \frac{4fL_k/V_{hub}}{(1 + 6fL_k/V_{hub})^{5/3}} \tag{14}$$

where $S_k(f)$ is the frequency dependent single sided velocity component spectrum, f is the frequency in Hertz, k is an index referring to the velocity component direction (1 = longitudinal, 2 = transverse, 3 = vertical), σ_k is the velocity component standard deviation and L_k is the velocity component integral scale parameter.

Fig. 2 presents a sample of a generated wind velocity time history with a prescribed mean value of zero and standard deviation of 2.29 m/s which is typical for mean wind speeds of 18 m/s with low turbulence characteristics [13]. A time step of 0.001 s was employed. The calculated mean and standard deviation of the resulting time series were 1.5×10^{-16} m/s and 2.25 m/s, respectively.

The standard [13] assumes that the longitudinal turbulence standard deviation σ_1 is invariant with height. In order to avoid over-complexity, uniform turbulence is assumed for the blades. This is justified by the fact that in the limit the result will not affect comparison of the relative performance of the systems considered in this study.

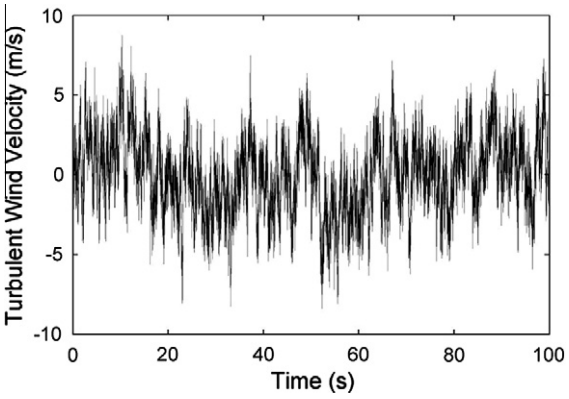

Fig. 2. Mean-removed wind velocity time history.

The specific nodal drag forces are computed for the blades. The modal drag forces for each particular mode i may subsequently be computed as:

$$F_{M,i}(t) = \phi_{T\_i}(z) \times F_D(t) \tag{15}$$

The loading on the tower is calculated in a similar fashion except the coherence of the fluctuating drag force component was taken account of by implementing a formulation proposed by Nigam and Narayanan [33] and successfully employed by Murtagh et al. [21] and Colwell and Basu [22]. This identifies the modal fluctuating drag force power spectrum, $S_{FjFj}(f)$, for a continuous line-like structure, which is discretised into a Multi Degree of Freedom (MDOF) dynamic system. It may be formulated as:

$$S_{FjFj}(f) = A(C_D\rho)^2 \sum_{k=1}^{n} \sum_{l=1}^{n} S_{VkVl}(f) \bar{v}_k \bar{v}_l \phi_j(k) \phi_j(l) \tag{16}$$

where k and l are discrete nodes, $S_{VkVl(f)}$, as outlined in Eq. (17), is the velocity auto PSDF when $k = l$ and the cross PSDF when $k \neq l$. $\bar{v}_k$ and $\bar{v}_l$ are the mean wind velocities at nodes k and l and $\phi_j(k)$ and $\phi_j(l)$ are the components of the jth modeshape which correspond to nodes k and l, respectively.

$$S_V kVl(f) = \sqrt{S_{V\_kk}(f) S_{V\_ll}(f)}\, coh(k,l;f) \tag{17}$$

$S_{V\_kk}(f)$ and $S_{V\_ll}(f)$ are the PSDFs at nodes k and l and may be calculated from the expression proposed by Kaimal et al. [12] and expressed as follows:

$$\frac{fS_{vv}(H,f)}{v_*^2} = \frac{200n}{(1 + 50n)^{5/3}} \tag{18}$$

The above equation is similar to Eq. (14) except for the addition of the variables H which is the height above the surface, v_* is the friction velocity calculated from Eq. (19) where k is the Von-karman constant and z_0 is the roughness length:

$$v(H) = \frac{1}{k} v_* \ln \frac{H}{z_0} \tag{19}$$

and n, which is expressed as:

$$n = \frac{fH}{\bar{v}(H)} \tag{20}$$

where $v(H)$ is the mean wind velocity at height H. The coherence function $coh(k,l;f)$ is represented as:

$$coh(k,l;f) = \exp\left[-\frac{|k-l|}{L_s} \right] \tag{21}$$

where $|k-l|$ is the spatial separation of the nodes and L_s is a length scale parameter given by:

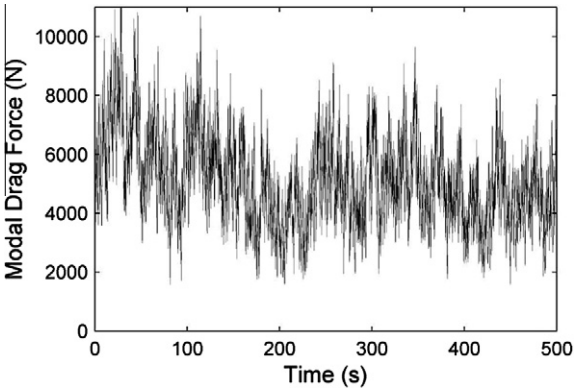

Fig. 3. Tower modal drag force time history for first mode.

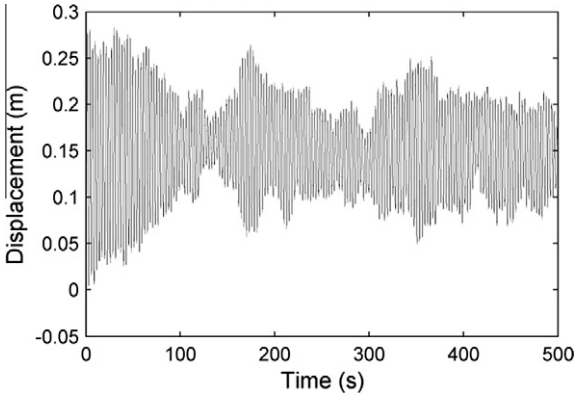

Fig. 4. Tower tip displacement for 500 s time interval.

$$L_s = \frac{\hat{v}}{fC} \tag{22}$$

with $\hat{v}$ being the average of the two mean wind speeds at k and l and C is a decay constant. The modal fluctuating drag force power spectrum may then be used to generate the modal fluctuating drag force time history for all relevant modes. The mean component may be calculated from Eq. (12) and the mean modal force is then determined by multiplying the result by the relevant modeshapes. Fig. 3 presents an example of a computed modal drag force time history for the first mode of vibration. The time history has a mean value of approximately 60 kN which is equal to the mean modal drag force and it exhibits a coefficient of variance (CoV) of approximately 5% of the mean which is close to the CoV of the wind velocity at the hub (6% of mean wind speed). The generated time histories account for the entire tower loading and allow for straightforward implementation in the modal form of the dynamic equation.

The system of equations outlined in Eq. (10) may then be solved once the equations have been formatted using a state-space formulation and the mass, damping, stiffness and force matrices are in modal form. The results of which are discussed in the following paragraphs.

By summing the displacement modal response for all modes of the tower and blades separately, the total displacement of the tip of the tower/blade may be calculated as a function of time. Fig. 4 shows a 500 s displacement time history of a typical tower subject to the modal drag force presented in Fig. 3. The analysis is carried out over 100 s time spans as this is considered sufficient to permit the complex system to stabilise as well as allowing sufficient time to perform a comparison of structural behaviour. The displacement response can be seen to oscillate about a mean positive displacement of approximately 0.15 m and after an initial maximum displacement just exceeding 0.25 m, the system gradually stabilises to a steady state. A probabilistic representation of these values is later presented to provide a comparison of the relative performance of the alternative tower configurations which are modelled.

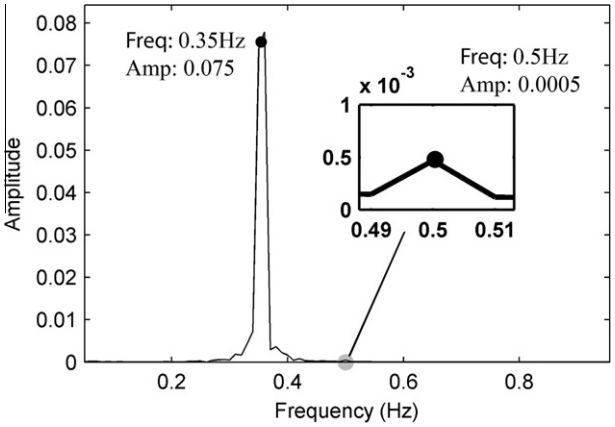

Fig. 5. Frequency response of tower tip displacements.

The frequency content of a displacement response time history is assessed to identify the important frequencies at which the tower responds. Fig. 5 displays a plot of the frequency content of the tower tip displacement shown in Fig. 4. These frequency plots are useful in that they allow validation of the performance of the model with respect to the incorporation of the system coupling. They also allow identification of the natural frequencies of the vibrating structural elements.

Two main peaks in energy occur in the system outlined in Figs. 3–5. The first at 0.35 Hz which corresponds closely to the natural frequency of the tower (0.33 Hz) and the second at 0.51 Hz which is the rotational speed of the blades applied to this particular simulation (0.5 Hz). This confirms that the system is operating correctly as the natural frequencies agree closely with those calculated previously and the coupling of the system is evident as the tower can be seen to exhibit some response at the rotational speed of the blades. Having validated the model for the base case, the focus can shift to the principal objective of this paper, i.e. comparison of the relative performance of concrete and steel tower solutions at varying heights.

3. Tower modelling

The objective of this work is to provide a comparison between the performance of steel and concrete wind turbine towers for a multi-megawatt turbine at hub heights in the range of 80–120 m. This problem is of interest to engineers due to the growing requirement to build taller support structures for larger multi-megawatt wind turbines. Two equivalent towers, constructed primarily of steel and concrete, respectively, are presented for the three specified hub heights of 90 m, 105 m and 122 m. These particular hub heights are chosen on the basis that they are at the upper end of current standard turbine heights and information such as structural properties were available for towers of these heights. In all cases the towers are assumed to support the NREL baseline 5-MW nacelle and rotor. The key properties of the turbine are listed in Table 1 [32].

Some further blade structural and aerodynamic properties are necessary for input to the model. These may be found in A. Relative comparison of the particular towers will be performed in terms of the maximum tip displacements for a series of prescribed wind regimes.

Table 1
Key properties of NREL baseline 5 MW wind turbine [32].

Property	Value
Rating	5 MW
Rotor diameter	126 m
Hub diameter	3 m
Cut-in wind speed	3 m/s
Rated wind speed	11.4 m/s
Cut-out wind speed	25 m/s
Cut-in rotor speed	6.9 rpm
Rated rotor speed	12.1 rpm
Nacelle mass	240,000 kg
Rotor mass	110,000 kg
Blade material	Glass-fibre
Blade length	61.5 m
Blade mass	17,740 kg
Blade CM (from blade root)	20.475 m
Blade damping ratio (all modes)	0.48%

3.1. Steel towers

Three tower heights are considered. The NREL 5-MW baseline onshore wind turbine tower [32] is considered for the 88 m tower, with a resulting 90 m hub height. The 103 m tower for the Vestas V-90 3 MW wind turbine [35,36] is scaled up to accommodate the additional mass of the 5 MW turbine unit, for an overall hub height of 105 m. Due to a lack of specification for the Vestas tower a number of properties and dimensions are assumed based on the available material. A third tower of 120 m is considered with a resulting tower height of 122 m. The properties of this tower are estimated from a scaling of the properties of the other two towers as no material was sourced for steel towers of this height. In all cases the tower diameter and steel thickness is assumed to taper linearly from bottom to top. Details of the key tower properties are outlined in Table 2. Further information on the tower properties as well as any assumptions made are provided in B. It should be noted that for each tower, the base diameter significantly exceeds 4.5 m and would, therefore, make them unsuitable for transport by road and notably difficult to manufacture.

3.2. Concrete towers

There is a lack of information in the literature relating to details of concrete wind turbine towers. This is due to the relatively recent emergence of prestressed concrete towers as an alternative to the more familiar steel towers. Therefore, in order to address heights equivalent to the steel tower heights it was decided to use the same base and top diameters as well as concrete thickness's for the two larger towers as for the 88 m tower, for which some basic properties were acquired. It is obvious that in reality this would not be the case and larger towers would utilise stiffer structures but in this instance any interpolation of tower properties to taller hub heights could not be verified by published material. The towers are assumed to have a circular cross-section the diameter of which tapers linearly from bottom to top, as with the steel towers. The concrete thickness is assumed to be constant throughout the height of the structure. Details of the key concrete tower properties are outlined in Table 3.

For the purposes of this comparative study the concrete towers considered are a lower-bound of realistic towers and represent conservative assumptions. This, in itself, will provide a means of comparing performance to the verified steel towers.

An important aspect of the analysis of the towers described above is to take appropriate consideration of the influence of the prestressing forces applied. The effect of prestress force on the dynamic performance of prestressed concrete elements is a topic which has been widely debated. The work of Hamed and Frostig [37], however, states that,"it has been mathematically rigorously proven that the magnitude of the prestressed force does not affect the natural frequencies of bonded or unbonded prestressed beams". Consequently, it is considered appropriate to discount the prestress force from the tower model and employ linear elastic beam theory in the analysis.

Table 2
Key properties of steel towers.

Property	Value		
	88 m Tower	103 m Tower	120 m Tower
Height	87.6 m	103 m	120 m
Base diameter	6 m	7.2 m	8.43 m
Base steel thickness	0.035 m	0.041 m	0.048 m
Top diameter	3.87 m	3.87 m	3.87 m
Top steel thickness	0.025 m	0.025 m	0.025 m
Young's modulus	Table 5	Table 5	Table 5
Steel density	Table 5	Table 5	Table 5
Total mass	356,620 kg	535,850 kg	798,640 kg
Location of CM (above base)	35.967 m	39.2 m	43.042 m
Tower damping ratio (all modes)	1%	1%	1%

Table 3
Key properties of concrete towers.

Property	Value		
	88 m Tower	103 m Tower	120 m Tower
Height	87.6 m	103 m	120 m
Base diameter	8.2 m	8.2 m	8.2 m
Top diameter	4.8 m	4.8 m	4.8 m
Concrete thickness	0.25 m	0.25 m	0.25 m
Young's modulus	Table 5	Table 5	Table 5
Steel density	Table 5	Table 5	Table 5
Total mass	1,053,500 kg	1,258,500 kg	1,466,300 kg
Location of CM (above base)	37.95 m	44.34 m	51.66 m
Tower damping ratio (all modes)	1%	1%	1%

3.3. Model implementation

Six mean hub-height wind speed values have been chosen as outlined in Table 4. The values specified lie within the normal operational range of multi-megawatt wind turbines, with 25 m/s being the usual cut-out wind speed [32,35,36]. In modelling the wind turbulence for the blades, the longitudinal standard deviation is given by a formula in BS EN 61400-1 [13]:

$$\sigma_1 = I_{ref}(0.75V_{hub} + b) \tag{23}$$

which accounts for a reference turbulence intensity I_{ref} and the mean wind speed at the hub V_{hub}. The reference turbulence intensity is specified based on whether the wind environment has low, medium or high turbulence characteristics. b is simply a factor equal to 5.6 m/s. In the case of the tower, the turbulence standard deviation is based on the friction velocity v_* which is a site specific parameter calculated from Eq. 19. As friction velocity is dependent on the mean wind speed at the hub-height, which is a variable in this study, only the values for σ_1 are specified for the varying mean hub-height wind speeds in Table 4.

The variables employed in the simulations, as characterised in Table 5, are probabilistic variables with specified probability density function (PDF) and CoV, excluding model uncertainty.

Table 4
Turbulence standard deviation at mean hub-height wind speeds.

Mean hub-height wind speed, $\overline{V}$(m/s)	16	18	20	22	24	25
σ_1 (m/s)						
Low turbulence	2.11	2.29	2.47	2.65	2.83	2.92
Medium turbulence	2.46	2.67	2.88	3.09	3.30	3.41
High turbulence	2.82	3.06	3.30	3.54	3.78	3.90

Table 5
Model input variables.

Tower material	Variable	Dimension	PDF	Mean (μ)	C.O.V. (%)	Refs.
Steel	E_s (Young's modulus)	(GPa)	LN	210	3	[32,38]
	ρ_s (Density)	(kg/m^3)	N	8500	1	[32,38]
	t_s (Thickness)	(mm)	N	varies	2	[38]
Concrete	E_c (Young's modulus)	(GPa)	LN	26	23	[39]
	ρ_c (Density)	(kg/m^3)	N	2450	4	[38]
	t_c (Thickness)	(mm)	N	varies	2	[38]
General	$\rho_a ir$ (air density)	(kg/m^3)	–	1.225	–	[13]
	k (Von-karman constant)	–	–	0.35	–	[40]
	z_0 (roughness length)	–	–	0.05	–	[2]

The values assigned to these variables are taken from previous research and design standards as referenced in the table.

A value of 1.2 is specified for the drag coefficient C_d of both towers [41].

3.4. Relative comparison of maximum tip displacements for varying hub heights

Fig. 6 presents the percentage variation in maximum tip displacements between the six towers modelled for varying wind speeds, where in the legend 'S' indicates the steel towers which are represented by solid lines and likewise 'C' is for concrete which have dotted lines. The points on the graph are the 95th percentile of the maximum displacement magnitudes at each wind speed. Only medium turbulence is considered in this instance.

The plot shows a distinct difference between the maximum displacements of the concrete and steel towers. As outlined previously, the 103 m and 120 m concrete towers are lower-bound estimates of realistic towers. Despite this, the 120 m concrete tower exhibits only 85% of the magnitude of the maximum displacement of the 120 m steel tower. This significant difference in magnitude is observed equally for the 88 m and 103 m towers with a consistent 15–20% difference in maximum displacement magnitude.

An almost linear increase in displacement magnitude is evident for all towers with increasing height. In the case of the steel towers, however, the rate of increase appears greater with increasing wind speed.

3.5. Long term effects in concrete

Prestressed concrete structures are subject to a number of effects which can alter their structural performance in the long term. Creep and shrinkage are two processes which must be considered in the long term design of concrete wind turbine towers. Both of these effects have the ability to induce tensile stresses which may lead to cracking of the concrete and a reduction in the overall strength of the structure. Numerous efforts have been made by

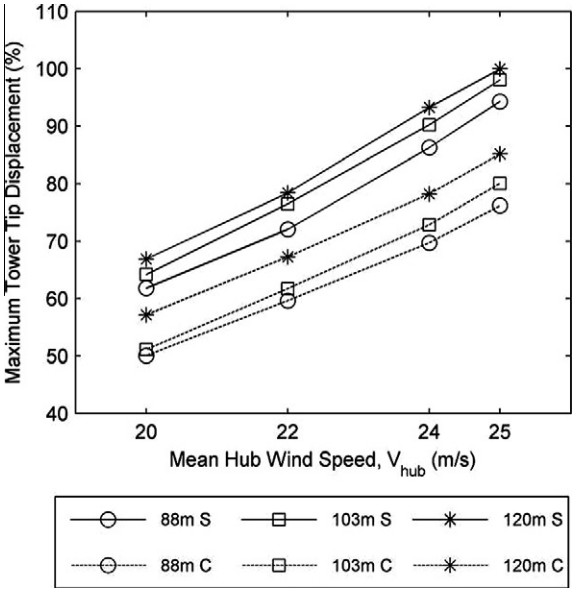

Fig. 6. Maximum tower tip displacements as a percentage of the overall maximum displacement for varying hub-heights and wind speeds with medium turbulence.

authors such as Cluley and Shepherd [42] and Mazloom [43] to quantify the effects of creep and shrinkage on the strength of prestressed concrete structures. Taking the approach outlined by Bazant and Whittmann [44] and utilising the formula:

$$J(t,t') = \frac{1+\phi(t,t')}{E(t')} \tag{24}$$

where $J(t,t')$ is a creep function, $\phi(t,t')$ is a creep coefficient and $E(t')$ is the modulus of elasticity at age t', it is possible to get an estimate of the reduced modulus of elasticity of the concrete after loading for time t. Considering that $J(t,t')$ is the strain at time t due to a unit constant stress that has been acting since time t' we can say that $1/J(t,t')$ is an approximation of the modulus of elasticity at time t. Taking the creep coefficient, $\phi(t,t')$, to be 1.0 and the modulus of elasticity, $E(t')$, to be 26 MPa (as per Table 5) we get a value for the adjusted modulus of elasticity of $E(t')/2$ or 13 MPa. Accounting for the effects of shrinkage and creep in this manner, a simulation will be undertaken to provide comparison to our standard results.

3.6. High strength concrete

As concrete wind turbine towers are considered to be high performance structures it would not be expected that normal grade prestressed concrete would be employed in their construction. It would be advisable that a high grade of concrete such as C50/60 (as specified in BS EN 206-1:2000 [45], with a characteristic compressive strength of 60 N/mm^2) or higher would be specified. This, in turn, would also have an influence on the modulus of elasticity (Young's Modulus) of the concrete as these two properties are known to be related. Noguchi et al. [46] proposed an equation for the modulus of elasticity of concrete with a specific relevance to high-strength concrete. This was formulated from over 3000 sets of experimental data and expresses the modulus of elasticity as:

$$E = k_1 k_2 \cdot 3.35 \times 10^4 (\gamma/2400)^2 (\sigma_B/60)^{1/3} \tag{25}$$

where E is the modulus of elasticity expressed in MPa, k_1 and k_2 are correction factors corresponding to aggregate coarseness and the addition of mineral admixtures respectively, γ is the unit weight

of the concrete expressed in kg/m^3 and σ_B is the concrete compressive strength expressed in MPa.

Taking, for example, a high-strength concrete with a mean unit weight of 2450 kg/m^3, as per Table 5, and characteristic compressive strength of 60 MPa will result in a modulus of elasticity of 34.91 GPa if we set both correction factors to 1.0. This is a significant increase on the mean value for Young's modulus specified for the concrete in Table 5. For comparison, a simulation will be carried out using the modulus of elasticity calculated above with the same distribution characteristics as specified in Table 5.

Furthermore, it would be expected that concrete wind turbine towers would be designed as Class 1 prestressed concrete structures which do not allow tensile forces to arise in the concrete under service loading. This would avoid any reduction in the strength of the structure in bending due to cracking of the concrete. Creep and shrinkage may still effect the concrete, however, so an additional simulation will be undertaken using an adjusted modulus of elasticity, as per Section 3.5, for the high strength concrete specified in this section.

4. Performance analysis using fragility curves

Fragility curves are most commonly used in seismic analysis as they provide an effective means of relating seismic hazard intensity to the probability of reaching or exceeding predefined limit states and are, therefore, a crucial ingredient in earthquake loss assessment. Ellingwood et al. [47] uses the theorem of total probability to outline the concept of seismic risk as follows:

$$P[Loss > c] = \sum_{s} \sum_{LS} \sum_{d} P[Loss > c|DS = d] \times P[DS = d|LS] \times P[LS|SI = s] \times P[SI = s] \quad (26)$$

where SI is the seismic intensity, measured in terms of ground motion (peak ground acceleration, velocity) or spectral (spectral acceleration, velocity or displacement) intensities, $P[LS|SI = s]$ is the probability of reaching a structural limit state LS, given the occurrence of $SI = s$, $P[DS = d|LS]$ is the probability of damage state DS, given limit state LS, and $P[Loss > c|DS = d]$ is the probability that the loss exceeds c, given that $DS = d$. $P[LS|SI = s]$ is known as the fragility term and it is in calculating this that fragility curves become valuable. In this study it is intended to employ fragility curves, which relate wind hazard intensity to a tower limit state, as a tool for comparing the relative structural performance of the wind turbine towers considered. A displacement based fragility curve generation procedure is utilised, based upon a limit state related to tower-tip displacement. Mean hub-height wind speed has been chosen as the fragility hazard parameter as it is quite straightforward and it dictates the underlying turbulent parameters of the wind speed. The fragility term employed in this analysis is represented as:

$$P\left[d_{tip} > LS|V_{hub} = \overline{V}\right] \quad (27)$$

where d_{tip} is the maximum tower tip displacement, LS is the tower limit state as specified below and V_{hub} is the mean hub-height wind speed.

The tower limit state for each tower height has been defined as the minimum extreme displacement of the tower tip for either the steel or concrete tower (whichever is the lesser) at the maximum mean hub-height wind velocity, 25 m/s.

5. Results

The output of the analysis outlined in the previous sections is in the form of tip displacements for the particular tower being examined. These results are presented in three formats. A comparison of the maximum tower tip displacements with respect to the varying hub heights was presented in Section 3.4. In this section a comparison of the tip displacements resulting from various turbulence levels are illustrated along with the presentation of a set of fragility curves, which describe the relative performance of concrete and steel towers at each particular hub-height.

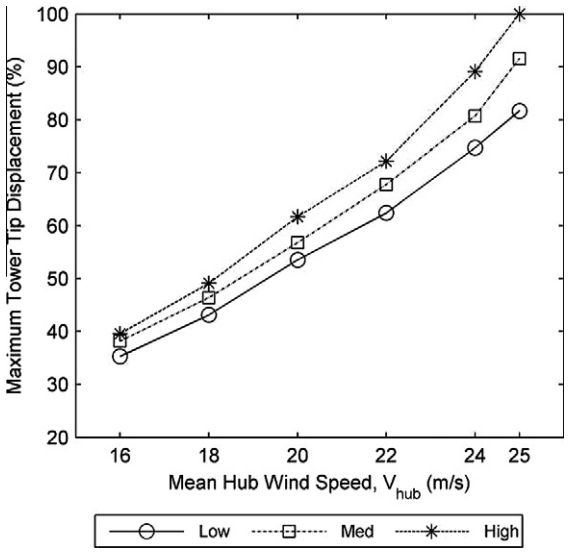

Fig. 7. Maximum tip displacements of 88 m steel tower with varying turbulence level.

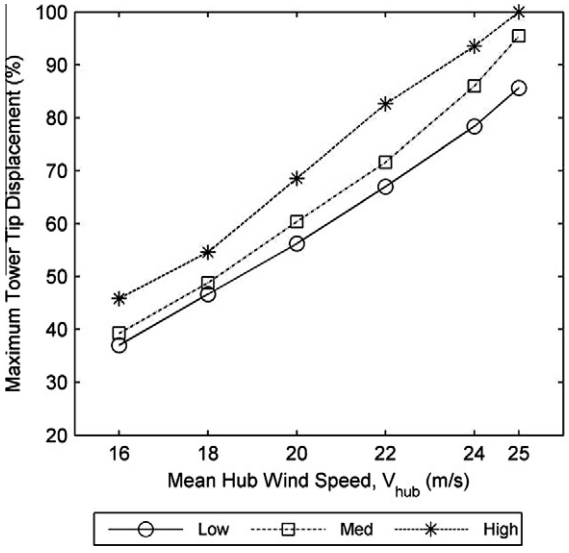

Fig. 8. Maximum tip displacements of 88 m concrete tower with varying turbulence level.

5.1. Comparison of maximum tower tip displacements for varying turbulence levels.

Figs. 7–12 outline the variation in maximum displacements of each tower studied for the three turbulence levels at the six mean hub-height wind speeds. In each case, 'Low', 'Med' and 'High' represent the displacements of the particular tower in conditions of low, medium or high turbulence, respectively. All three turbulence levels are investigated in order to certify that variation in turbulence levels affects both the steel and concrete towers equally.

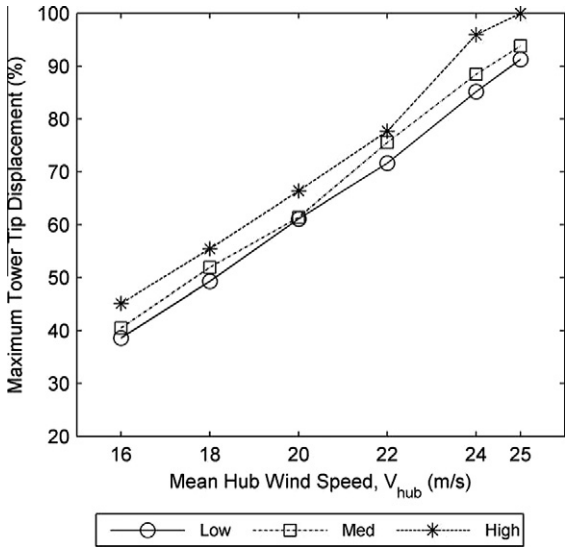

Fig. 9. Maximum tip displacements of 103 m steel tower with varying turbulence level.

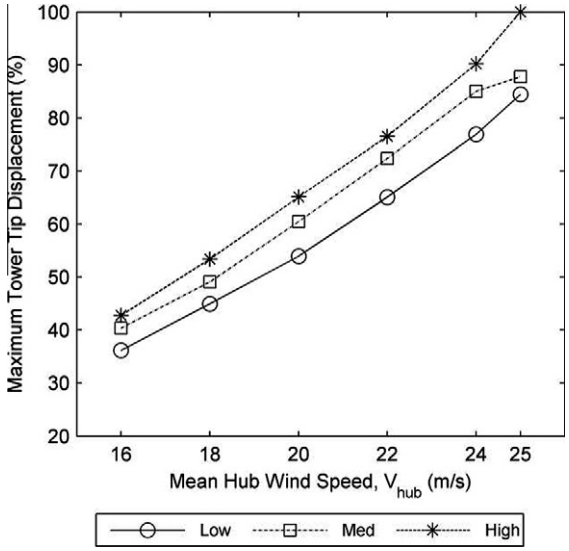

Fig. 10. Maximum tip displacements of 103 m concrete tower with varying turbulence level.

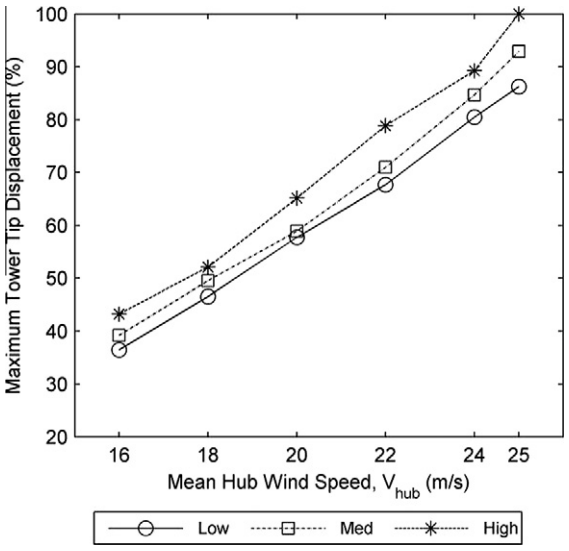

Fig. 11. Maximum tip displacements of 120 m steel tower with varying turbulence level.

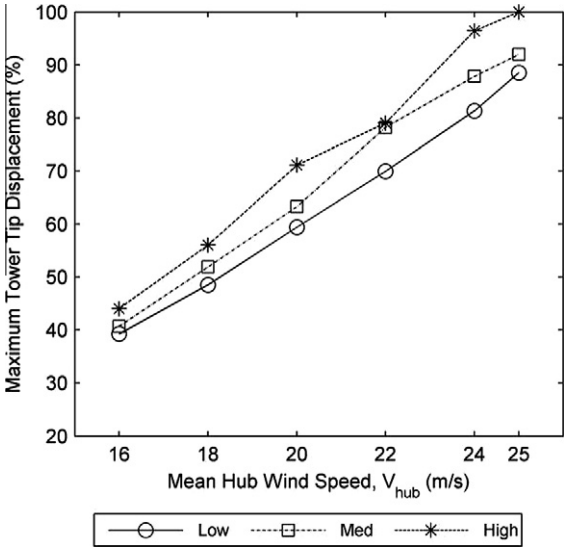

Fig. 12. Maximum tip displacements of 120 m concrete tower with varying turbulence level.

The displacements are characterised as a percentage of the maximum displacements for that particular tower.

It is evident that there is a distinct increase in maximum tip displacements with increasing turbulence for both steel and concrete towers, as would be expected, but as the tower height increases the separation of the magnitudes appears less defined as can be seen in Figs. 11 and 12. There is no clear pattern which effects either of the two tower materials in solitude. In what follows, the comparison of the performance of the two materials is presented for one turbulence level only.

5.2. Fragility curves

Figs. 13–15 illustrate a set of fragility curves which outline the relative performance of the two tower materials at the three heights specified. Only the case of medium turbulence is considered as the effect of turbulence has already been addressed in Section 5.1. In each graph the probability of exceeding the limit state is defined on the *y*-axis as described in Section 4 while the *x*-axis defines the mean hub-height wind speed.

A consistent disparity is evident between the results for the two tower materials in all three figures indicating the superior structural performance of the specified concrete towers as opposed to their steel counterparts for the considered limit state. Despite the fact that the diameter and material thickness properties for the two taller concrete towers are the same as the 88 m tower, Figs. 13–15 demonstrate the considerably lower probabilities of limit state exceedance of the concrete towers for all three hub heights. This is seen to be most significant at higher wind speeds. Fig. 15 does show a reduction in the disparity between the two tower materials but this is to be expected given that the 120 m tall concrete tower is specified with the properties of a typical 88 m tower whereas the 120 m steel tower is scaled from the 103 m and 88 m towers. Fig. 6 echoes these findings with a clear distinction between the maximum displacements of the steel and concrete

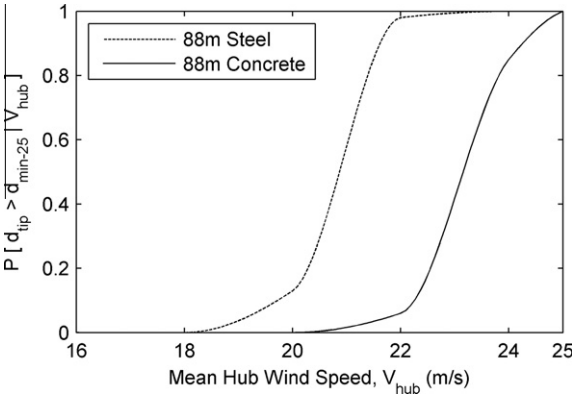

Fig. 13. Fragility curves for 88 m steel and concrete towers.

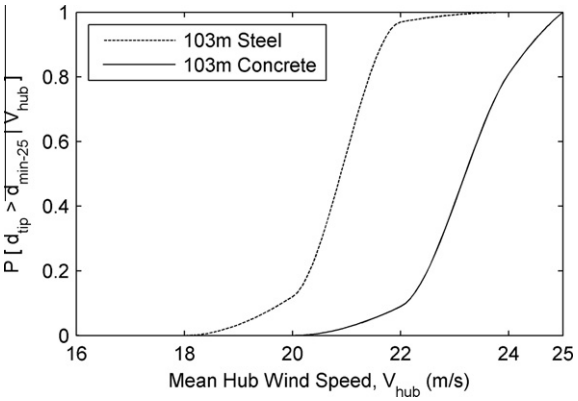

Fig. 14. Fragility curves for 103 m steel and concrete towers.

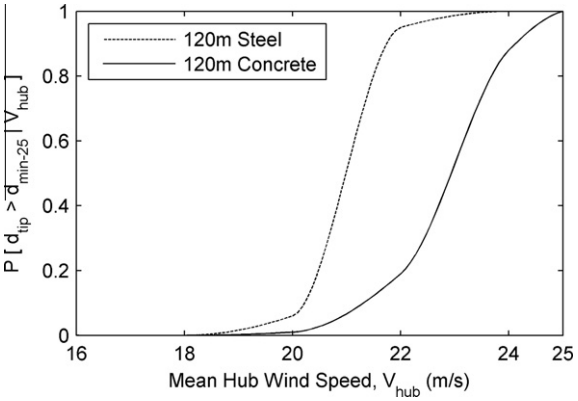

Fig. 15. Fragility curves for 120 m steel and concrete towers.

towers. It can be seen that the 120 m concrete tower, which again is a lower-bound to a realistic tower of this height, exhibits between 5% and 10% lower displacements than the 88 m steel tower.

Fig. 16 is the same as Fig. 15 but with the addition of a third curve. This curve represents the probability of limit state exceedance for a 120 m concrete tower which incorporates a reduction in strength due to long term effects, creep and shrinkage. The properties of the concrete are for standard grade and not high strength concrete. There is a clear decrease in performance from the original concrete tower. It can be seen that the aged tower behaves in a similar fashion to the steel tower with slightly inferior performance up to 21 m/s mean wind speed but improved performance

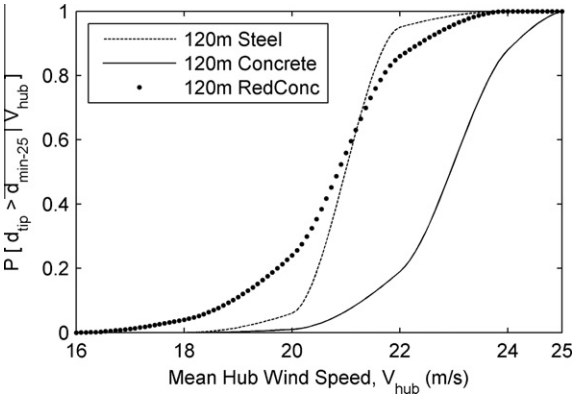

Fig. 16. Fragility curves for 120 m steel and concrete towers with a concrete tower modelled with long term effects.

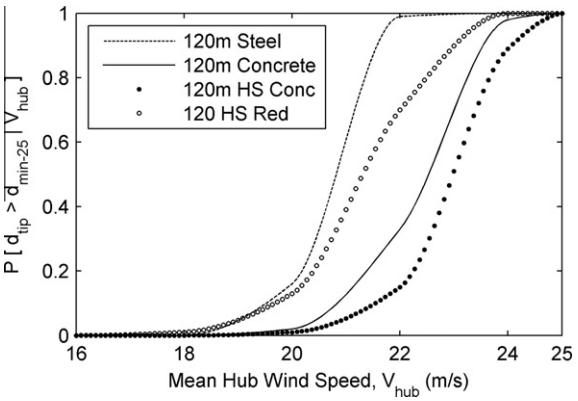

Fig. 17. Fragility curves for 120 m steel and concrete towers with a high strength concrete tower.

beyond this speed. Below 20 m/s the performance of the three towers appears to converge

Fig. 17 presents a set of fragility curves for a 120 m tower constructed from a high strength concrete compared to the standard 120 m steel and concrete tower. An additional curve has been added for a standard high strength concrete prestressed structure along with a curve representing the same tower incorporating long term effects. As expected, the high strength concrete tower clearly displays improved performance over the original concrete tower as well as the reference steel tower. When long term effects are taken into account the performance is below the standard concrete tower but it still maintains improved performance over the steel tower, with increasing benefit as wind speeds increase.

6. Conclusion

This paper set out to compare the relative structural performance of steel and prestressed concrete wind turbine towers for heights ranging from 88 m to 120 m. A Lagrangian formulation was employed to develop a dynamic model of the wind turbine system. This ensured all elements of coupling and centrifugal stiffening were incorporated. Turbulent wind loading was simulated by the summation of mean and fluctuating components at specific nodes on the tower and blades. Both steel and concrete towers were modelled for the hub heights considered. The parameters of these towers were defined as probabilistic variables.

Maximum tower tip displacements were utilised in comparing relative structural performance of the various towers. The effect

of increasing the level of turbulence on the towers was investigated. Varying the turbulence level was seen to have a noticeable effect on the magnitudes of maximum tip displacements. However, this was observed to effect both tower types equally with no evident pattern exclusive to either material. Fragility curves were employed to directly compare the performance of the two tower materials. The limit state was defined as the lowest maximum tip displacement for either tower at each specific height. For all cases it was seen that the steel towers exhibited significantly higher probabilities of limit state exceedance. Despite the fact that the prestressed concrete towers defined were particularly conservative, they none the less performed better than the steel alternatives in terms of limit state exceedance. A basic model of long term effects in prestressed concrete, such as creep and shrinkage, was developed in order to simulate tower performance in the long term. When these effects were taken into account for a 120 m tall tower it was observed that the steel and concrete tower showed minimal difference in performance with steel exhibiting superior results at lower wind speeds but a reversal of performance was observed at higher wind speeds. As details on concrete specification for these structures were unavailable it was decided to specify regular strength concrete for the simulations. However, it would be expected that a high strength concrete would be prescribed for these high performance structures. The simulation of a high strength concrete in a 120 m tall tower was observed to induce a distinct and uniform improvement over regular strength concrete and, therefore, the steel option as would be expected. The inclusion of long term effects in the simulation reduced this improvement but the tower remained significantly ahead of the steel option in terms of reduced probability of limit state exceedance.

Steel wind turbine towers have been the predominant solution used in the wind industry thus far. The results in this paper suggest that prestressed concrete towers can provide a viable alternative and offer improved performance. As was evident in the results, the magnitude of the improvement is dependent on the type of concrete specified. Even with the standard grade concrete, however, the towers demonstrated much improved performance based on the design parameters and despite there being minimal difference in results in the long term the possibility of far greater life spans for concrete towers [48] gives concrete a distinct advantage over the steel option. This will be particularly beneficial to future projects where hub heights will increase resulting in the manufacturing and transport problems associated with current steel tower designs.

Acknowledgements

Partial funding by Banagher Precast Concrete Ltd under the IRCSET (Irish Research Council for Science, Engineering & Technology) Enterprise Partnership Scheme is gratefully acknowledged.

Appendix A

Table 6 contains additional blade structural properties used in the wind turbine model. The ‘‘Radius’’ column outlines the distance of each point on the blade from the rotor centre, ‘‘BlFract’’ represents the fractional distance of each node from the root of the blade, ‘‘BMassDen’’ is the mass density of the blade at each particular node and ‘‘FlpStiff’’ is the structural stiffness, ‘‘EI’’, of each blade at each particular node.

Table 7 contains additional blade aerodynamic properties used in the wind turbine model. The ‘‘Node’’ column outlines the number of each node along the blade, ‘‘RNodes’’ represents the distance of each node along the blade from the rotor centre, ‘‘DRNodes’’ is

Table 6
Distributed blade structural properties [32].

Radius (m)	BlFract (−)	BMassDen (kg/m)	FlpStiff (Nm^2)
1.50	0.00000	709.7315	18.11E+09
1.70	0.00325	709.7315	18.11E+09
2.70	0.01951	808.4427	19.43E+09
3.70	0.03577	774.1413	17.46E+09
4.70	0.05203	773.6103	15.29E+09
5.70	0.06829	619.3716	10.78E+09
6.70	0.08455	470.6994	7.23E+09
7.70	0.10081	443.2890	6.31E+09
8.70	0.11707	418.8109	5.53E+09
9.70	0.13335	399.3923	4.98E+09
10.70	0.14959	417.7833	4.94E+09
11.70	0.16585	445.6589	4.69E+09
12.70	0.18211	435.7269	3.95E+09
13.70	0.19837	424.6105	3.39E+09
14.70	0.21465	398.7212	2.93E+09
15.70	0.23089	368.8260	2.57E+09
16.70	0.24715	365.3293	2.39E+09
17.70	0.26341	362.2570	2.27E+09
19.70	0.29595	354.7251	2.05E+09
21.70	0.32846	344.9730	1.83E+09
23.70	0.36098	336.5955	1.59E+09
25.70	0.39350	328.0549	1.36E+09
27.70	0.42602	308.1031	1.10E+09
29.70	0.45855	300.1438	8.76E+08
31.70	0.49106	275.2882	6.81E+08
33.70	0.52358	264.6925	5.35E+08
35.70	0.55610	252.6280	4.09E+08
37.70	0.58862	230.6461	3.15E+08
39.70	0.62115	209.3783	2.37E+08
41.70	0.65366	187.5418	1.76E+08
43.70	0.68618	172.5827	1.26E+08
45.70	0.71870	161.4151	1.07E+08
47.70	0.75122	145.2371	9.09E+07
49.70	0.78376	135.4316	7.63E+07
51.70	0.81626	112.1295	6.11E+07
53.70	0.84878	103.2565	4.95E+07
55.70	0.88130	94.3416	3.94E+07
56.70	0.89756	86.7659	3.47E+07
57.70	0.91382	76.2130	3.04E+07
58.70	0.93008	71.8915	2.65E+07
59.20	0.93821	69.2697	2.38E+07
59.70	0.94636	62.0317	1.96E+07
60.20	0.95447	58.4503	1.60E+07
60.70	0.96260	54.8647	1.28E+07
61.20	0.97073	51.3418	1.01E+07
61.70	0.97886	47.8963	7.55E+06
62.20	0.98699	43.5591	4.60E+06
62.70	0.99512	11.9725	2.50E+05
63.00	1.00000	10.7871	1.70E+05

Table 7
Distributed blade aerodynamic properties [32].

Node (−)	RNodes (m)	DRNodes (m)	Chord (m)
1	2.8667	2.733	3.542
2	5.6000	2.733	3.854
3	8.3333	2.733	4.167
4	11.7500	4.1000	4.557
5	15.8500	4.1000	4.652
6	19.9500	4.1000	4.458
7	24.0500	4.1000	4.249
8	28.1500	4.1000	4.007
9	32.2500	4.1000	3.748
10	36.3500	4.1000	3.502
11	40.4500	4.1000	3.256
12	44.5500	4.1000	3.010
13	48.6500	4.1000	2.764
14	52.7500	4.1000	2.518
15	56.1667	2.7333	2.313
16	58.9000	2.7333	2.086
17	61.6333	2.7333	1.419

Table 8
Distributed properties of equivalent on-shore tower for NREL 5 MW baseline wind turbine [32].

Elevation (m)	Ht_Fract (−)	Mass_Den (kg/m)	FA_Stiff (Nm^2)
0.00	0.0	5575	614E+09
8.76	0.1	5274	535E+09
17.52	0.2	4973	463E+09
26.28	0.3	4673	399E+09
35.04	0.4	4372	342E+09
43.80	0.5	4071	291E+09
52.56	0.6	3770	246E+09
61.32	0.7	3469	206E+09
70.08	0.8	3169	172E+09
78.84	0.9	2868	142E+09
87.60	1.0	2567	116E+09

Table 9
Distributed properties of scaled 103 m steel tower.

Elevation (m)	Ht_Fract (−)	Mass_Den (kg/m)	FA_Stiff (Nm^2)
0.00	0.0	7838	1.24E+12
10.30	0.1	7311	1.13E+12
20.60	0.2	6784	1.02E+12
30.90	0.3	6257	9.04E+11
41.20	0.4	5730	7.91E+11
51.50	0.5	5202	6.79E+11
61.80	0.6	4675	5.67E+11
72.10	0.7	4148	4.54E+11
82.40	0.8	3621	3.42E+11
92.70	0.9	3094	2.30E+11
103.0	1.0	2567	1.17E+11

Table 10
Distributed properties of scaled 120 m steel tower.

Elevation (m)	Ht_Fract (−)	Mass_Den (kg/m)	FA_Stiff (Nm^2)
0.00	0.0	10744	2.33E+12
12.0	0.1	9926	2.11E+12
24.0	0.2	9108	1.89E+12
36.0	0.3	8290	1.67E+12
48.0	0.4	7473	1.45E+12
60.0	0.5	6655	1.22E+12
72.0	0.6	5838	1.00E+12
84.0	0.7	5020	7.81E+11
96.0	0.8	4202	5.60E+11
108.0	0.9	3385	3.39E+11
120.0	1.0	2567	1.17E+11

the length of blade associated with each particular node and "Chord" is the chord length at each particular node.

Appendix B

B.1. 88 m Steel tower – distributed properties

Table 8 presents the distributed mass and stiffness properties of the NREL baseline 5 MW wind turbine equivalent on-shore tower, as Specified by Jonkman et al. [32]. Note that 'Elevation' signifies the vertical elevation above the tower base, 'Ht_Fract' represents the fractional height of each particular node, 'Mass_Den' is the mass density of the tower at the particular node and 'FA_Stiff' stands for the forward-aft (flapwise direction for blades) stiffness of the tower at the particular node.

B.2. 103m Steel tower – distributed properties

The total mass of the components supported by the standard 103 m tower is 112 metric tonnes for the Vestas 3 MW turbine [36]. This represents 32% of the mass of the 5 MW baseline turbine specified for this study. The top and bottom diameters of the tower are, therefore, scaled up by 68% to give the values specified in Table 2. The base steel thickness is estimated as the thickness of the 88 m tower (0.035 m) scaled up by a factor of 18% which represents the increase in height. The distributed properties used to model the 103 m steel tower are presented in Table 9.

Table 11
Distributed properties of 88 m concrete tower.

Elevation (m)	Ht_Fract (−)	Mass_Den (kg/m)	FA_Stiff (Nm^2)
0.00	0.0	15682	1.38E+12
8.76	0.1	14990	1.27E+12
17.52	0.2	14297	1.15E+12
26.28	0.3	13604	1.04E+12
35.04	0.4	12912	9.26E+11
43.80	0.5	12219	8.12E+11
52.56	0.6	11526	6.98E+11
61.32	0.7	10833	5.84E+11
70.08	0.8	10141	4.69E+11
78.84	0.9	9448	3.55E+11
87.60	1.0	8755	2.41E+11

Table 12
Distributed properties of 103 m concrete tower.

Elevation (m)	Ht_Fract (−)	Mass_Den (kg/m)	FA_Stiff (Nm^2)
0.00	0.0	15682	1.38E+12
10.30	0.1	14990	1.27E+12
20.60	0.2	14297	1.15E+12
30.90	0.3	13604	1.04E+12
41.20	0.4	12912	9.26E+11
51.50	0.5	12219	8.12E+11
61.80	0.6	11526	6.98E+11
72.10	0.7	10833	5.84E+11
82.40	0.8	10141	4.69E+11
92.70	0.9	9448	3.55E+11
103.0	1.0	8755	2.41E+11

Table 13
Distributed properties of 120 m concrete tower.

Elevation (m)	Ht_Fract (−)	Mass_Den (kg/m)	FA_Stiff (Nm^2)
0.00	0.0	15682	1.38E+12
12.0	0.1	14990	1.27E+12
24.0	0.2	14297	1.15E+12
36.0	0.3	13604	1.04E+12
48.0	0.4	12912	9.26E+11
60.0	0.5	12219	8.12E+11
72.0	0.6	11526	6.98E+11
84.0	0.7	10833	5.84E+11
96.0	0.8	10141	4.69E+11
108.0	0.9	9448	3.55E+11
120.0	1.0	8755	2.41E+11

B.3. 120 m Steel tower – distributed properties

No tower has been found in literature against which to model the 120 m steel tower. As a result, the properties of this tower are estimated from scaling the 103 m Vestas tower and the 88 m NREL tower. The change in hub-height elevation from the 103 m tower represents a 17% increase in tower height. The base diameter and steel thickness are consequently increased by 17%. The distributed properties used to model the 120 m steel tower are presented in Table 10.

B.4. Concrete towers – distributed properties

The properties of the 88 m concrete tower are established from a typical tower of this height. No literature could be found detailing

the properties and dimensions of concrete towers in the range of 100 m to 120 m. It was, therefore, decided to use the same properties for the taller towers as for the 88 m tower, except for the height. The diameters and concrete thickness of the taller towers would obviously be greater in reality but these towers will provide a lower-bound with which to compare the steel counterparts. The distributed properties used to model the three concrete towers are presented in Tables 11–13.

References

[1] Windblatt. Enercon Mag Wind Energy 2010;04(1).
[2] Hau E. Wind turbines: fundamentals, technologies, applications, economics. 2nd ed. Berlin: Springer; 2006.
[3] Irish road traffic (construction and use of vehicles) (amendment) regulations. Office of the Attorney General; 2008.
[4] Virlogeux M. Der viadukt ++ber das tarntal bei millau G von den ersten entwurfsgedanken bis zur fertigstellung. Bautechnik 2006;83(2):85–107.
[5] Windblatt. Enercon Mag Wind Energy 2010:03.
[6] Garrad A. Dynamics of wind turbines: physical science, measurement and instrumentation, management and education – reviews. IEE Proc A 1983;130(9):523–30.
[7] Sorensen JD, Toft HS. Probabilistic design of wind turbines. Energies 2010;3:241–57.
[8] Toft HS, Sorensen JD. Reliability-based design of wind turbine blades. Struct Safety; in press, Corrected Proof.
[9] Due+as-Osorio L, Basu B. Unavailability of wind turbines due to wind-induced accelerations. Eng Struct 2008;30(4):885–93.
[10] Harte R, Van Zijl GPAG. Structural stability of concrete wind turbines and solar chimney towers exposed to dynamic wind action. J Wind Eng Ind Aerodyn 2007;95(9–11):1079–96.
[11] Mann J. Wind field simulation. Probab Eng Mech 1998;13(4):269–82.
[12] Kaimal JC, Wyngaard JC, Izumi Y, Cot+ OR. Spectral characteristics of surface layer turbulence. Quart J R Meteorol Soc 1972;98:563–89.
[13] Wind turbines-part 1: design requirements. British Standards Institution; 2005.
[14] Madsen PH, Frandsen S. Wind-induced failure of wind turbines. Eng Struct 1984;6(4):281–7.
[15] Connell JR. The spectrum of wind speed fluctuations encountered by a rotating blade of a wind energy conversion system. Solar Energy 1982;29(5):363–75.
[16] Veers P. Three-dimensional wind simulation. Sandia National Laboratories; 1988.
[17] Bazeos N, Hatzigeorgiou GD, Hondros ID, Karamaneas H, Karabalis DL, Beskos DE. Static, seismic and stability analyses of a prototype wind turbine steel tower. Eng Struct 2002;24(8):1015–25.
[18] Chen Xb, Li J, Chen Jy. Wind-induced response analysis of a wind turbine tower including the blade-tower coupling effect. J Zhejiang Univ – Sci A 2009;10(11):1573–80.
[19] Negm HM, Maalawi KY. Structural design optimization of wind turbine towers. Comput Struct 2000;74(6):649–66.
[20] Lee D, Hodges DH, Patil MJ. Multi-flexible-body dynamic analysis of horizontal axis wind turbines. Wind Energy 2002;5(4):281–300.
[21] Murtagh PJ, Basu B, Broderick BM. Along-wind response of a wind turbine tower with blade coupling subjected to rotationally sampled wind loading. Eng Struct 2005;27(8):1209–19.
[22] Colwell S, Basu B. Tuned liquid column dampers in offshore wind turbines for structural control. Eng Struct 2009;31(2):358–68.
[23] Murtagh PJ, Basu B, Broderick BM. Mode acceleration approach for rotating wind turbine blades. In: Proceedings of the institution of mechanical engineers – Part K. Journal of Multi-body Dynamics, vol. 218. 2004a. p. 159–67.
[24] Nigam N, Jennings P. Digital calculation of response spectra from strong motion earthquake records. Tech. Rep.. California Institute of Technology; 1968.
[25] Hansen MH. Improved modal dynamics of wind turbines to avoid stall-induced vibrations. Wind Energy 2003;6(2):179–95.
[26] Arrigan J. Semi-active vibration control of wind turbine blades using a time-frequency approach, Ph.D. thesis. The University of Dublin, Trinity College; 2010.
[27] Arrigan J, Pakrashi V, Basu B, Nagarajaiah S. Control of flapwise vibrations in wind turbine blades using semi-active tuned mass dampers. Structural Control and Health Monitoring; 2010.
[28] Clough RW, Penzien J. Dynamics of structures. Singapore: McGraw-Hill; 1993.
[29] Naguleswaran S. Lateral vibration of a centrifugally tensioned uniform Euler–Bernoulli beam. J Sound Vib 1994;176(5):613–24.
[30] Naguleswaran S. Out-of-plane vibration of a uniform Euler–Bernoulli beam attached to the inside of a rotating rim. J Sound Vib 1997;200(1):63–81.
[31] Ozgumus O, Kaya M. Flapwise bending vibration analysis of double tapered rotating Euler–Bernoulli beam by using the differential transform method. Meccanica 2006;41(6):661–70.
[32] Jonkman J, Butterfield S, Musial W, Scott G. Definition of a 5-mw reference wind turbine for offshore system development. Tech. Rep.. National Renewable Energy Laboratory; 2009.
[33] Nigam N, Narayanan S. Applications of random vibrations. Delhi: Springer-Verlag; 1994.
[34] Murtagh PJ, Basu B, Broderick BM. Wind force time-history generation by discrete fourier transform (dft). In: Multi-body dynamics – monitoring and simulation Techniques – lll. John Wiley & Sons; 2004b.
[35] Vestas. General specification, v90 – 3 mw, 2004.
[36] Vestas. General specification, v90 – 1.8/2 mw (optispeed G wind turbine), 2005.
[37] Hamed E, Frostig Y. Natural frequencies of bonded and unbonded prestressed beams – prestress force effects. J Sound Vib 2006;295(1–2):28–39.
[38] Vrouwenvelder T. The JCSS probabilistic model code. Struct Safety 1997;19(3):245–51.
[39] Kong F, Evans R. Reinforced and prestressed concrete. 3rd ed. Cambridge: Spon Press; 1987.
[40] Businger JA, Wyngaard JC, Izumi Y, Bradley EF. Flux–profile relationships in the atmospheric surface layer. J Atmospheric Sci 1971;28:181–9.
[41] Simiu E, Scanlan RH. Wind effects on structures: fundamentals and applications to design. 3rd ed. New York: John Wiley & Sons; 1996.
[42] Cluley N, Shepherd R. Analysis of concrete cable-stayed bridges for creep, shrinkage and relaxation effects. Comput Struct 1996;58(2):337–50.
[43] Mazloom M. Estimating long-term creep and shrinkage of high-strength concrete. Cement Concrete Compos 2008;30(4):316–26.
[44] Bazant ZP, Whittmann FH. Creep and shrinkage in concrete structures. Wiley; 1982.
[45] Concrete-part 1: specification, performance, production and conformity. British Standards Institution; 2000.
[46] Noguchi T, Tomosawa F, Nemati KM, Chiaia BM, Fantilli AP. A practical equation for elastic modulus of concrete. Am Concrete Inst – Struct J 2009;106(5):690–6.
[47] Ellingwood BR, Celik OC, Kinali K. Fragility assessment of building structural systems in mid-America. Earthquake Eng Struct Dyn 2007;36(13):1935–52.
[48] Tricklebank AH, Halberstadt PH, Magee BJ, Bromage A. Concrete towers for onshore and offshore wind farms. Tech. Rep.. The Concrete Centre; 2007.